Journal of Computational and Applied Research in Mechanical Engineering
jcarme.sru.ac.ir
SRTTU
JCARME
ISSN: 2228-7922

The increasing electrical response of piezoelectric nonlinear plate in harmonic excitation with strain nodes

Majid Jabbari

Department of Mechanical Engineering, Khomeinishahr Branch, Islamic Azad University, Khomeinishahr/Isfahan, Iran

Article info:

Article history:

Received: 00/00/0000
Accepted: 00/00/0018
Revised: 00/00/0000
Online: 00/00/0000

Keywords:
Electrical,
Piezoelectric,
Multilayered,
Mindlin,
Nonlinear.

***Corresponding author:**
jabbari@iaukhsh.ac.ir

Abstract

Electrical energy can be harvested from the vibrations of piezoelectric plates. The behavior of the piezoelectric plate is simulated using electromechanical coupling. Given the large strain experienced by the flexible plate, the linear theory is inadequate; therefore, the effect of Von Karman strain must be considered. This paper investigates and validates the vibrational behavior of a piezoelectric nonlinear plate. Specifically, it employs coupled equations for a multilayered plate, incorporates Von Karman's nonlinear strain, and applies Mindlin's first-order shear deformation theory. The electrical response is obtained through finite element analysis of the piezoelectric nonlinear plate in Matlab. Different boundary conditions are considered to verify the results, including clamped edges, simply supported edges, and a combination of two simply supported and two clamped edges. The electrical response of the open-circuit case under harmonic excitation is presented. Furthermore, the phenomenon of voltage cancellation during plate vibrations is studied, and a method for enhancing energy harvesting performance using separated electrodes is proposed. The results indicate that, across all cases, the voltage response with a continuous electrode is lower than with segmented electrodes at the first natural frequency.

1. Introduction

Energy harvesting from the vibration of piezoelectric structures has garnered significant attention in recent years. Hausler *et al.* 0investigated the first test results of the energy harvesting from piezoelectric materials.
Lallart *et al.* 0presented the technique of self-tuning including automatic frequency actuation and detection that a technique of tuning stiffness uses to change the frequency of the piezoelectric harvester to set the source vibrations. Erturk and Inman 0 studied energy harvesting in piezoelectric beam. In the paper, Euler-Bernoulli, Rayleigh, and Timoshenko beam theories was be used in the assumed-modes method. Erturk and Inman 0presented the mathematical model of piezoelectric beam for harvester.
These piezoelectric energy harvesters can predict the coupled dynamics behaviour. Erturk

0proposed the analytical solution of an energy harvesting piezoelectric beam under the excitation of harmonic base. This method of solution presented the accurate result of piezoelectric harvester behavior.

Finite element method was applied to the simulation of piezoelectric materials behavior in variable researches. Jabbari *et al.* 0proposed modeling of a harvester using a piezoelectric multilayer beam. They presented a numerical and experimental method for harvesting energy from a piezoelectric multilayer nonlinear beam under harmonic loading.

The element of smart structure was presented by Bucalem and Kogl 0. Then the element was applied by Lazarus and Crawley. Bendigeri *et al.* 0presented the finite element model of the piezoelectric material. A hexahedral element of eight noded was applied to the coupling behavior of the electromechanical structure.

In this study, the piezoelectric property effects were presented by a finite element model. Sebald *et al.* 0 presented a technique that excite the jumping systems to the solution of high amplitude in the harvester of piezoelectric broadband. Piefort and Preumont 0used shell element of Mindlin as the piezoelectric structures.

Erturk and Inman 0studied the response of chaotic on high energy orbit for an oscillator of duffing and the coupling of electro-mechanical. Van den Ende 0has developed the formulation for the mechanical and piezoelectric properties of lead-zirconate-titanate and LCR.

The polymer piezoelectric property is greatly affected by temperature. This materials present proper processing ability for the conditions of high temperature. The excellent thermal resistances of polymers make those a proper material for application of industrial.

Brian *et al.* 0investigated piezoelectric materials. They showed when stress is applied to piezoelectric structure, this material produces the voltage of self actuated. Jabbari *et al.* 0investigated the simulation and test results of vibration analysis of a piezoelectric cantilever beam.

In the paper, the effect of piezoelectric on the electric and dynamic responses was obtained. Then the velocity effect and the concentrated mass position on the electric response were studied. Ng and Lio 0 presented the behavior of a unimorph cantilever harvester connected to piezoelectric element in the parallel and series conditions.

Lazarus *et al.* 0proposed the numerical method for the vibration of piezoelectric beam and NEMS. Xu *et al.* [17, 18] applied the coefficient of '33'mode for piezoelectric harvester. In the paper, it was presented that the electrical power for "31" mode is more than the "31" mode piezoelectric coefficient.

Kaltenbacher 0researched numerical model for the hysteresis loops of polarization field and butterfly curve of piezoelectric structures. Bintang and Yudong 0showed the modeling of piezoelectric nonlinear actuator and the properties of piezoelectric actuator. Jabbari 0proposed increasing the performance of energy harvesting in vibration mode shapes.

They presented a method of design for the harvester of a cantilever piezoelectric beam. In this method, they apply the segmented electrode avoided the voltage cancellations in the vibrations. Kong *et al.* 0investigated the electromechanical coupling the delivering load to the impedance and complex load.

It was presented that 75% efficiency should be expressed to the conjugate coupling loads with the frequency of narrow band. Xu *et al.* 0 proposed the energy harvester using a multilayer stack of PZT. In the work, it was applied the "33" mode of a piezoelectric harvester.

They presented that the capacitance property and multilayer piezoelectric structure depend on the dynamic behavior. Nurettin Sezer and Muammer 0presented a comprehensive review on the state-of-the-art of piezoelectric energy harvesting.

The piezoelectric energy conversion principles were delineated, and the working mechanisms and operational modes of piezoelectric generators were elucidated. Xiaotian Zheng *et al.* 0 presented a comprehensive review of state-of-the-art advances in piezoelectric wind energy harvesters (PWEH).

Han *et al.* 0 introduce flexible amorphous thin-film energy harvesters based on perovskite $CaCu_3Ti_4O_{12}$ (CCTO) thin films on a plastic substrate for highly competitive electromechanical energy harvesting.

Givois *et al.* 0 investigated the nonlinear resonant behavior of piezoelectric plates through experimental analysis, focusing on how geometric nonlinearities affect the vibrational and electromechanical responses of these plates. Shariati *et al.*0 showed that the damping coefficient is responsible of the bifurcation point variation, while the amplitude response depends on the term of the natural frequency.

The previous studies related to the current research are prepared in a Table 1.

Table 1. The previous studies.

Ref.	Authors/year	Aim of research
1	Hausler et al./1984.	the first test results of the energy harvesting from piezoelectric materials
2	Lallart et al./2010	technique of self-tuning including automatic frequency actuation and detection
3, 4	Erturk and Inman/2010,2011	the mathematical model of piezoelectric beam for harvester
5	Erturk/2009	the analytical solution of an energy harvesting piezoelectric beam
6	Jabbari et al./2017	modeling of a harvester using a piezoelectric multilayer beam
7	Bucalem and Kogl/2005	The element of smart structure
8	Bendigeri et al./2011	the finite element model of the piezoelectric material
9	Sebald et al./2011	a technique that excite the jumping systems to the solution of high amplitude in the harvester of piezoelectric broadband
10	Piefort and Preumont/2000	shell element of Mindlin as the piezoelectric structures
11	Erturk and Inman/2011	the response of chaotic on high energy orbit for an oscillator of duffing and the coupling of electro-mechanical
12	Van den Ende/2007	the formulation for the mechanical and piezoelectric properties of lead-zirconate-titanate and LCR
13	Brian et al./2005	Investigation of piezoelectric materials
14	Jabbari et al./2015	the simulation and test results of vibration analysis of a piezoelectric cantilever beam
15	Ng and Lio/2005	the behavior of a unimorph cantilever harvester connected to piezoelectric element
16	Lazarus et al./2012	the numerical method for the vibration of piezoelectric beam and NEMS
17 18	NEMS . Xu et al./2012,2013	the coefficient of '33'mode for piezoelectric harvester.
19	Kaltenbacher/ 2010	numerical model for the hysteresis loops of polarization field
20	Bintang and Yudong/2012	the modeling of piezoelectric nonlinear actuator
21	Jabbari/2017	increasing the performance of energy harvesting in vibration mode shapes
22	Kong et al./2010	the electromechanical coupling the delivering load to the impedance and complex load
23	Xu et al./2013	the energy harvester using a multilayer stack of PZT
24	Muammer/2021	a comprehensive review on the state-of-the-art of piezoelectric energy harvesting
25	Xiaotian Zheng et al./2023	a comprehensive review of state-of-the-art advances in piezoelectric wind energy harvesters
26	Han et al./2024	flexible amorphous thin-film energy harvesters based on perovskite $CaCu_3Ti_4O_{12}$ (CCTO) thin films
27	Givois et al./2020	the nonlinear resonant behavior of piezoelectric plates through experimental analysis
28	Shariati et al./2021	the damping coefficient is responsible of the bifurcation point variation, while the amplitude response depends on the term of the natural frequency

In this research, the electrical response of the open circuit case in harmonic excitation and energy harvesting in resonance excitation are obtained. Also the increasing of energy harvesting performance is presented by using the separated electrodes.

In the paper, the Mindlin theory for the Von Karman strain and the first order shear deformation for nonlinear geometry are applied (Fig. 1).

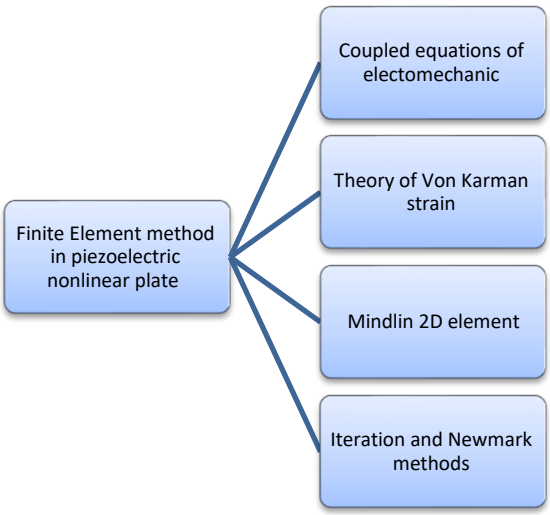

Fig. 1. The algorithm of finite element method.

2. Theoretical formulation

The Mindlin theory is applied to analyze thick plates. This theory assumes that the in-plane displacement varies linearly through the thickness, and the transverse displacement remains constant. Unlike classical plate theory, the Mindlin theory accounts for shear deformation; therefore, a normal plane on the plate surface remains plane after deformation, but is not necessarily normal to the deformed mid-surface. The displacement field in the Mindlin theory is defined as follows:

$$u(x,y,z,t) = u_o(x,y,t) - z\,\theta_x(x,y,t)$$

$$v(x,y,z,t) = v_o(x,y,t) - z\,\theta_y(x,y,t)$$

$$w(x,y,z,t) = w_o(x,y,t) \qquad (1)$$

Where u, is displacement along x axis, v, displacement along y axis and w, displacement along z axis, u_o, v_o and w_o, midplane displacement, θ_x and θ_y, rotation of y and x axis, respectively (Fig. 2).

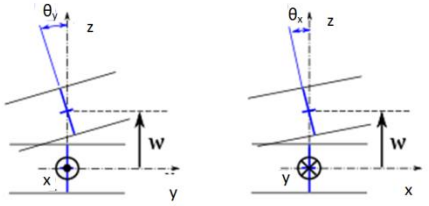

Fig. 2. The displacement and rotation parameters.

Green-Lagrangian strain vector is used in the Mindlin theory and the Von Karman parameter is applied in the nonlinear effect of strain. The strain equations are presented as follow0:

$$\varepsilon_x = \frac{\partial u}{\partial x} + \frac{1}{2}\left(\frac{\partial w}{\partial x}\right)^2 = \frac{\partial u_o}{\partial x} - z\frac{\partial \theta_x}{\partial x} + \frac{1}{2}\left(\frac{\partial w_o}{\partial x}\right)^2 = \{\varepsilon_{x_o}\} - z\{\vartheta_x\} + \{\varepsilon_x^N\} \quad (2)$$

$$\varepsilon_y = \frac{\partial v}{\partial y} + \frac{1}{2}\left(\frac{\partial w}{\partial y}\right)^2 = \frac{\partial v_o}{\partial y} - z\frac{\partial \theta_y}{\partial y} + \frac{1}{2}\left(\frac{\partial w_o}{\partial y}\right)^2 = \{\varepsilon_{y_o}\} - z\{\vartheta_y\} + \{\varepsilon_y^N\}$$

$$\gamma_{xy} = \frac{\partial u}{\partial y} + \frac{\partial v}{\partial x} + \frac{\partial w}{\partial x}\frac{\partial w}{\partial y} = \frac{\partial u_o}{\partial y} + \frac{\partial v_o}{\partial x} - z\frac{\partial \theta_x}{\partial y} - z\frac{\partial \theta_y}{\partial x} + \frac{\partial w_o}{\partial x}\frac{\partial w_o}{\partial y}$$

$$= \{\varepsilon_{x_o}\} + \{\varepsilon_{y_o}\} - z\{\vartheta_{xy}\} + \{\varepsilon_{xy}^N\}$$

$$\gamma_{yz} = \frac{\partial v}{\partial z} + \frac{\partial w}{\partial y} = \frac{\partial w_o}{\partial y} - \theta_y$$

$$\gamma_{xz} = \frac{\partial u}{\partial z} + \frac{\partial w}{\partial x} = \frac{\partial w_o}{\partial x} - \theta_x \quad (3)$$

Where ε_x and ε_y, are the inplane longitude strains, γ_{yz} and γ_{xz}, the transverse shear strains, γ_{xy}, inplane shear strain. The strain vector is obtained as follow:

$$\begin{Bmatrix} \varepsilon_x \\ \varepsilon_y \\ \gamma_{xy} \end{Bmatrix} = \{\varepsilon_o\} - z\{\vartheta\} + \{\varepsilon_N\} \qquad \begin{Bmatrix} \gamma_{yz} \\ \gamma_{xz} \end{Bmatrix} = \{\varepsilon_s\} \quad (4)$$

$$\{\varepsilon_o\} = \begin{Bmatrix} \varepsilon_{x_o} \\ \varepsilon_{y_o} \\ \gamma_{xy_o} \end{Bmatrix} = \begin{bmatrix} \frac{\partial}{\partial x} & 0 \\ 0 & \frac{\partial}{\partial y} \\ \frac{\partial}{\partial y} & \frac{\partial}{\partial x} \end{bmatrix} \begin{Bmatrix} u_o \\ v_o \end{Bmatrix} = [D_\varepsilon] \begin{Bmatrix} u_o \\ v_o \end{Bmatrix} \quad (5)$$

$$\{\vartheta\} = \begin{Bmatrix} \vartheta_x \\ \vartheta_y \\ \vartheta_{xy} \end{Bmatrix} = \begin{bmatrix} \frac{\partial}{\partial x} & 0 \\ 0 & \frac{\partial}{\partial y} \\ \frac{\partial}{\partial y} & \frac{\partial}{\partial x} \end{bmatrix} \begin{Bmatrix} \theta_x \\ \theta_y \end{Bmatrix} = [D_\vartheta] \begin{Bmatrix} \theta_x \\ \theta_y \end{Bmatrix} \quad (6)$$

$$\{\varepsilon_N\} = \begin{Bmatrix} \varepsilon_x^N \\ \varepsilon_y^N \\ \gamma_{xy}^N \end{Bmatrix} = \frac{1}{2}\begin{bmatrix} \frac{\partial w_o}{\partial x} & 0 \\ 0 & \frac{\partial w_o}{\partial y} \\ \frac{\partial w_o}{\partial y} & \frac{\partial w_o}{\partial x} \end{bmatrix} \begin{Bmatrix} \frac{\partial}{\partial x} \\ \frac{\partial}{\partial y} \end{Bmatrix} w_o \quad (7)$$

$$= \frac{1}{2}[\Gamma_\theta(w)]\{D_N\} w_o$$

$$\{\varepsilon_s\} = \begin{Bmatrix} \frac{\partial w_o}{\partial y} - \theta_y \\ \frac{\partial w_o}{\partial x} - \theta_x \end{Bmatrix} = \begin{bmatrix} \frac{\partial}{\partial y} & 0 & -1 \\ \frac{\partial}{\partial x} & -1 & 0 \end{bmatrix} \begin{Bmatrix} w_o \\ \theta_x \\ \theta_y \end{Bmatrix}$$

$$= \begin{bmatrix} \{D_w\} & -[I_s] \end{bmatrix} \begin{Bmatrix} w_o \\ \theta_x \\ \theta_y \end{Bmatrix} \quad (8)$$

$$[I_s] = \begin{bmatrix} 0 & 1 \\ 1 & 0 \end{bmatrix}$$

Where $\{\varepsilon_o\}$, is midplane strain vector, $\{\vartheta\}$, curvature vector, $\{\varepsilon_N\}$, nonlinear strain vector, $\{\varepsilon_S\}$, vector of transverse shear strain.

The coupled equations for a layer i of a multilayered plate are presented as follow:

$$\{D\}_j = [\bar{e}]_i \{\varepsilon\}_j + [\mu]_j \{E\}_j$$

$$\{\sigma\}_j = [K]_j \{\varepsilon\}_j - [\bar{e}]_j^T \{E\}_j \quad (9)$$

Where $\{\varepsilon\}$, is the Green Lagrangian strain vector $\{\sigma\}$, the second Piola Kirchoff stress vector, $\{D\}$, the vector of electric displacement, $[\mu]$, the electric field vector, $[\bar{e}]$, the piezoelectric matrix, $[K]$, the permittivity matrix,$\{E\}$, the stiffness matrix.

The piezoelectric coefficients e_{34} and e_{35} are zero because it is purposed that no shear force in zx and yz planes is excited by using the electrical field.

The constitutive equations are expands as follows.

$$\begin{Bmatrix} D_x \\ D_y \\ D_z \end{Bmatrix}_j = \left[\begin{array}{ccc:cc} 0 & 0 & 0 & \bar{e}_{14} & \bar{e}_{15} \\ 0 & 0 & 0 & \bar{e}_{24} & \bar{e}_{25} \\ \hdashline \bar{e}_{31} & \bar{e}_{32} & \bar{e}_{36} & 0 & 0 \end{array}\right]_j \begin{Bmatrix} \varepsilon_x \\ \varepsilon_y \\ \gamma_{xy} \\ \hdashline \gamma_{yz} \\ \gamma_{xz} \end{Bmatrix}_j \quad (10)$$

$$+ \left[\begin{array}{cc:c} \mu_{11} & \mu_{12} & 0 \\ \mu_{12} & \mu_{22} & 0 \\ \hdashline 0 & 0 & \mu_{33} \end{array}\right]_j \begin{Bmatrix} E_x \\ E_y \\ \hdashline E_z \end{Bmatrix}_j$$

$$\begin{Bmatrix}\sigma_x\\ \sigma_y\\ \tau_{xy}\\ \tau_{yz}\\ \tau_{xz}\end{Bmatrix}_j = \left[\begin{array}{ccc:cc} K_{11} & K_{12} & K_{16} & 0 & 0\\ K_{12} & K_{22} & K_{26} & 0 & 0\\ K_{16} & K_{26} & K_{66} & 0 & 0\\ \hdashline 0 & 0 & 0 & K_{44} & K_{45}\\ 0 & 0 & 0 & K_{45} & K_{55}\end{array}\right]_j \begin{Bmatrix}\varepsilon_x\\ \varepsilon_y\\ \gamma_{xy}\\ \gamma_{yz}\\ \gamma_{xz}\end{Bmatrix} - \left[\begin{array}{ccc:cc} 0 & 0 & 0 & \bar{e}_{14} & \bar{e}_{15}\\ 0 & 0 & 0 & \bar{e}_{24} & \bar{e}_{25}\\ \hdashline \bar{e}_{31} & \bar{e}_{32} & \bar{e}_{36} & 0 & 0\end{array}\right]_j^T \begin{Bmatrix}E_x\\ E_y\\ E_z\end{Bmatrix}_j \quad (11)$$

The vector of electric field is defined by using the electric potential φ as follow:

$$\begin{Bmatrix}E_x\\ E_y\\ E_z\end{Bmatrix} = -\begin{Bmatrix}\frac{\partial\varphi}{\partial x}\\ \frac{\partial\varphi}{\partial y}\\ \frac{\partial\varphi}{\partial z}\end{Bmatrix} = -\begin{Bmatrix}\frac{\partial}{\partial x}\\ \frac{\partial}{\partial y}\\ \frac{\partial}{\partial z}\end{Bmatrix}\varphi(x,y,z) = -\{\nabla_\varphi\}\varphi(x,y,z) \quad (12)$$

The electric potential changes linearity through the thickness of the plate layers. So its value is presented as follow.

$$\begin{aligned}\varphi^\rho(x,y,z) &= \left(\frac{z-z_\rho}{t_\rho}\right)\varphi_t^\rho(x,y) + \left(\frac{z_{\rho+1}-z}{t_\rho}\right)\varphi_b^\rho(x,y)\\ &= \left[M_{\varphi1}^\rho(z) \quad M_{\varphi2}^\rho(z)\right]\begin{Bmatrix}\varphi_b^\rho(x,y)\\ \varphi_t^\rho(x,y)\end{Bmatrix}\end{aligned} \quad (13)$$

$$\left[M_\varphi^\rho(z)\right] = \left[M_{\varphi1}^\rho(z) \quad M_{\varphi2}^\rho(z)\right]$$

$$\{\varphi^\rho(x,y)\} = \begin{Bmatrix}\varphi_b^\rho(x,y)\\ \varphi_t^\rho(x,y)\end{Bmatrix}$$

$$M_{\varphi1}^\rho(z) = \left(\frac{z_{\rho+1}-z}{t_\rho}\right) \quad M_{\varphi2}^\rho(z) = \left(\frac{z-z_\rho}{t_\rho}\right)$$

Where φ_t^ρ and φ_b^ρ are the electric potential at the top and bottom of the piezoelectric layer ρ, t_ρ, the thickness of layer ρ.

$$\{E\}_\rho = -\{\nabla_\varphi\}\left[M_\varphi^\rho(z)\right]\{\varphi^\rho(x,y)\} = -[Z_\varphi^\rho][D_\varphi^\rho]\{\varphi^\rho(x,y)\}$$

$$[Z_\varphi^\rho] = \begin{bmatrix} M_{\varphi1}^\rho & M_{\varphi2}^\rho & 0 & 0 & 0 & 0\\ 0 & 0 & M_{\varphi1}^\rho & M_{\varphi2}^\rho & 0 & 0\\ 0 & 0 & 0 & 0 & -1/t_\rho & 1/t_\rho\end{bmatrix} \quad (14)$$

$$[D_\varphi^\rho] = \begin{bmatrix} \frac{\partial}{\partial x} & 0 & \frac{\partial}{\partial y} & 0 & 1 & 0\\ 0 & \frac{\partial}{\partial x} & 0 & \frac{\partial}{\partial y} & 0 & 1\end{bmatrix}^T \quad (15)$$

The stress equations for a layer ρ of a multilayer plate can be expressed as follow:

$$\begin{Bmatrix}\{\sigma_p\}\\ \{\sigma_s\}\end{Bmatrix}_\rho = \left[\begin{array}{c:c}[K_p] & [0]\\ \hdashline [0] & [K_s]\end{array}\right]_\rho \begin{Bmatrix}\{\varepsilon_p\}\\ \{\varepsilon_s\}\end{Bmatrix}_\rho + \left[\begin{array}{c:c}[0] & [\bar{e}_s]\\ \hdashline [\bar{e}_p] & [0]\end{array}\right]_\rho^T [Z_\varphi^\rho][D_\varphi^\rho]\{\varphi^\rho(x,y)\} \quad (16)$$

$$[\bar{e}_p] = [\bar{e}_{31} \ \bar{e}_{32} \ \bar{e}_{36}] \quad [\bar{e}_s] = \begin{bmatrix}\bar{e}_{14} & \bar{e}_{15}\\ \bar{e}_{24} & \bar{e}_{25}\end{bmatrix}$$

$$[K_p] = \begin{bmatrix}K_{44} & K_{45}\\ K_{45} & K_{55}\end{bmatrix} \quad [K_s] = \begin{bmatrix}K_{11} & K_{12} & K_{16}\\ K_{12} & K_{22} & K_{26}\\ K_{16} & K_{26} & K_{66}\end{bmatrix}$$

Where $[K_S]$, is the transverse shear stiffness matrix, $[K_\rho]$, the inplane stress stiffness matrix. The electric displacement equations for a layer ρ of a multilayer plate can be expressed as follow:

$$\begin{Bmatrix}\{D_s\}\\ D_p\end{Bmatrix}_\rho = \left[\begin{array}{c:c}[0] & [\bar{e}_s]\\ \hdashline [\bar{e}_p] & [0]\end{array}\right]_\rho \begin{Bmatrix}\{\varepsilon_p\}\\ \{\varepsilon_s\}\end{Bmatrix}_\rho - \left[\begin{array}{c:c}[\mu_s] & \{0\}\\ \hdashline [0] & \mu_p\end{array}\right]_\rho [Z_\varphi^\rho][D_\varphi^\rho]\{\varphi^\rho(x,y)\} \quad (17)$$

The above equation presents the results of stress per unit width of the plate (Fig. 3).

$$\begin{aligned}&(\{N\},\{M\},\{T\})\\ &= \int_{-h/2}^{+h/2}\left(\{\sigma_p\}, z\{\sigma_p\}, \{\sigma_s\}\right)dz\end{aligned} \quad (18)$$

$$\{M\} = \begin{Bmatrix}M_x\\ M_y\\ M_{xy}\end{Bmatrix} \{N\} = \begin{Bmatrix}N_x\\ N_y\\ N_{xy}\end{Bmatrix} \{T\} = \begin{Bmatrix}T_{yz}\\ T_{xz}\end{Bmatrix}$$

Where {N}, is the vector of inplane stress, {M}, the vector of moment, {T}, the vector of transverse shear stress, h, is the plate thickness. By using the above equations, the following relatives are obtained.

$$\begin{Bmatrix}\{N\}\\ \{M\}\end{Bmatrix}=\begin{bmatrix}[A] & [B]\\ [B] & [D]\end{bmatrix}\begin{Bmatrix}\{\varepsilon^o\}+\{\varepsilon_N\}\\ \{\vartheta\}\end{Bmatrix}+\begin{bmatrix}[A_e]^T\\ [B_e]^T\end{bmatrix}\{\hat{\varphi}\} \tag{19}$$

$$\{T\}=[S]\{\varepsilon_s\}+[S_e^1]^T\frac{\partial}{\partial x}\{\hat{\varphi}\}+[S_e^2]^T\frac{\partial}{\partial y}\{\hat{\varphi}\} \tag{20}$$

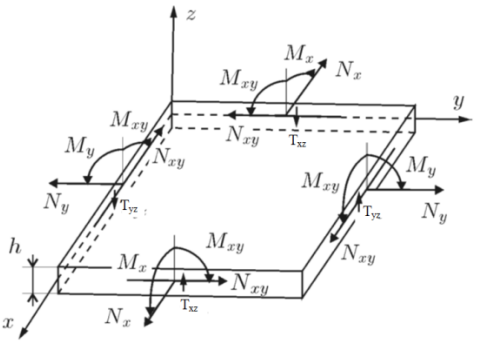

Fig. 3. The stress of mindlin plate.

The equation of strain-displacement can be defined as follow:

$$\begin{aligned}
&\{\varepsilon_b\}=\{\varepsilon_b^L\}+\{\varepsilon^N\}=\left[[D_b^L]+\tfrac{1}{2}[D^N(w)]\right]\{\hat{u}\}\\
&\{\varepsilon_b^L\}=\begin{Bmatrix}\{\varepsilon_o\}\\ \{\vartheta\}\end{Bmatrix}\quad\{\varepsilon^N\}=\begin{Bmatrix}\{\varepsilon_N\}\\ \{0\}\end{Bmatrix}\\
&[D_b^L]=\begin{bmatrix}[D_\varepsilon] & \{0\}_{3x1} & [0]_{3x2}\\ [0]_{3x2} & \{0\}_{3x1} & [D_\vartheta]\end{bmatrix}\\
&[D^N(w)]=\begin{bmatrix}[0]_{3x2} & [\Gamma_\theta(w)]\{D_N\} & [0]_{3x2}\\ [0]_{3x2} & \{0\}_{3x1} & [0]_{3x2}\end{bmatrix}\\
&\{\hat{u}\}=\begin{bmatrix}u_o & v_o & w_o & \theta_x & \theta_y\end{bmatrix}^T\\
&\{\varepsilon^s\}=[D_s]\{\hat{u}\}\\
&[D_s]=\begin{bmatrix}[0]_{2x2} & \{D_w\} & -[I_2]\end{bmatrix}
\end{aligned} \tag{22}$$

The vector of inplane stress-moment and the transverse shear stress are expressed as follow:

$$\{\bar{N}\}=[C]([D_b^L]+\tfrac{1}{2}[D^N(w)])\{\hat{u}\}+[C_e]^T\{\hat{\varphi}\}=\begin{Bmatrix}\{N\}\\ \{M\}\end{Bmatrix}=\{\bar{N}^u\}+\{\bar{N}^\varphi\} \tag{23}$$

$$\{T\}=[S]\{\varepsilon_s\}+[S_e]^T[D_\varphi]\{\hat{\varphi}\}=\{T^u\}+\{T^\varphi\} \tag{24}$$

$$\begin{Bmatrix}\{\bar{N}^i\}\\ \{M^i\}\end{Bmatrix}=\begin{Bmatrix}\{N^i\}\\ \{M^i\}\end{Bmatrix}\quad\{N^i\}=\begin{Bmatrix}N_x^i\\ N_y^i\\ N_{xy}^i\end{Bmatrix} \tag{25}$$

$$\{M^i\}=\begin{Bmatrix}M_x^i\\ M_y^i\\ M_{xy}^i\end{Bmatrix}\quad\{T^i\}=\begin{Bmatrix}T_{yz}^i\\ T_{xz}^i\end{Bmatrix}\quad i=u,\varphi$$

$$\begin{aligned}
&[S_e]^T=\begin{bmatrix}[S_e]_1^T & [S_e]_2^T & \cdots & [S_e]_{NP}^T\end{bmatrix}\\
&[S_e]_\rho^T=\begin{bmatrix}[S_e^1]_\rho^T & [S_e^2]_\rho^T & [0]\end{bmatrix}\\
&[S_e^1]_\rho=\frac{t_\rho}{2}\begin{bmatrix}\bar{e}_{14} & \bar{e}_{15}\\ \bar{e}_{14} & \bar{e}_{15}\end{bmatrix}_\rho\\
&[S_e^2]_k=\frac{t_\rho}{2}\begin{bmatrix}\bar{e}_{24} & \bar{e}_{25}\\ \bar{e}_{24} & \bar{e}_{25}\end{bmatrix}_\rho
\end{aligned} \tag{26}$$

The vector of electric potential and the gradient matrix of electric potential for multilayer plate are presented in the following relative.

$$\{\hat{\varphi}\}=\begin{Bmatrix}\begin{Bmatrix}\varphi_b^1\\ \varphi_t^1\end{Bmatrix}\\ \vdots\\ \begin{Bmatrix}\varphi_b^{NP}\\ \varphi_t^{NP}\end{Bmatrix}\end{Bmatrix}\quad[D_\varphi]=\mathrm{diag}\left[[D_\varphi^1]\ \ [D_\varphi^2]\ \ \cdots\ \ [D_\varphi^{NP}]\right] \tag{27}$$

The coefficient matrixes of multilayer plate are obtained as follow:

$$[C]=\begin{bmatrix}[A] & [B]\\ [B] & [D]\end{bmatrix}\ ([A],[B],[D])=\sum_{k=1}^{NL}[K_p]_k\left((z_{k+1}-z_k),\tfrac{1}{2}(z_{k+1}^2-z_k^2),\tfrac{1}{3}(z_{k+1}^3-z_k^3)\right) \tag{28}$$

$$\begin{aligned}
&[C_e]^T=\begin{bmatrix}[A_e]^T\\ [B_e]^T\end{bmatrix}\\
&[A_e]^T=\begin{bmatrix}[A_e]_1^T & [A_e]_2^T\cdots[A_e]_{NP}^T\end{bmatrix}\\
&[A_e]_\rho=\begin{Bmatrix}-1\\ 1\end{Bmatrix}\{\bar{e}_p\}_\rho^T\\
&[B_e]^T=\begin{bmatrix}[B_e]_1^T & [B_e]_2^T\cdots[B_e]_{NP}^T\end{bmatrix}\\
&[B_e]_\rho=\frac{1}{2}(z_{\rho+1}+z_\rho)[A_e]_\rho\\
&[S]=[F_s]\sum_{i=1}^{NL}[K_s]_k(z_{k+1}-z_k)[F_s]\\
&[F_s]=\begin{bmatrix}f_s & 0\\ 0 & f_s\end{bmatrix}
\end{aligned} \tag{29, 30}$$

Where NL, is the total number of layers, NP, the piezoelectric layers number.

The correction factor f_s is presented by follow equation, because the transverse shear stress changes in the thickness direction 0.

$$f_s=\left(\frac{8\lambda^2 IC_c}{(1-\upsilon)Ah^2\rho}\right)\quad A=\int_{-\frac{h}{2}}^{\frac{h}{2}}\frac{C_c}{1-\upsilon^2}x^2dx\quad \lambda^2=\frac{h^2}{4}\frac{\rho_0}{C_c}\omega^2 \tag{31}$$

Where C_c, is the elasticity module, λ, the frequency parameter, ω, the vibration frequency of transverse shear, ρ_0, the plate density, υ, the poison factor.
The mechanical energy can be defined by the elastic and piezoelectric stress as follow:

$$\Pi^M=\frac{1}{2}\int_V\{\varepsilon_p\}^T\{\sigma_p^u\}dV+\frac{1}{2}\int_V\{\varepsilon_p\}^T\{\sigma_p^\varphi\}dV+\frac{1}{2}\int_V\{\varepsilon_s\}^T\{\sigma_s^u\}dV+\frac{1}{2}\int_V\{\varepsilon_s\}^T\{\sigma_s^\varphi\}dV \tag{32}$$

Where Π^M, is Hellinger Reissner function, V, the plate volume, $\{\varepsilon_p\}$, the vector of plane strain, $\{\varepsilon_S\}$, the vector of transverse shear strain, $\{\sigma_p{}^u\}$, the vector of elastic stress, $\{\sigma_p{}^\varphi\}$, the vector of piezoelectric stress, $\{\sigma_s{}^u\}$, the vector of elastic transverse shear stress, $\{\sigma_s{}^\varphi\}$, the vector of piezoelectric transverse shear stress.
The volume integral is replaced to the surface integral by the vector of inplane stress-moment.

$$\Pi^M=\frac{1}{2}\int_A\{\varepsilon_b\}^T\{\bar{N}^u\}dA+\frac{1}{2}\int_A\{\varepsilon_b\}^T\{\bar{N}^\varphi\}dA+\frac{1}{2}\int_A\{\varepsilon_s\}^T\{T^u\}dA+\frac{1}{2}\int_A\{\varepsilon_s\}^T\{T^\varphi\}dA \tag{33}$$

The follow equation is obtained by the coefficient matrix.

$$\Pi^M=\frac{1}{2}\int_A\{\varepsilon_b\}^T[C]\{\varepsilon_b\}dA+\frac{1}{2}\int_A\{\varepsilon_b\}^T[C_e]^T\{\bar{\varphi}\}dA+\frac{1}{2}\int_A\{\varepsilon_s\}^T[S]\{\varepsilon_s\}dA+\frac{1}{2}\int_A\{\varepsilon_s\}^T[S_e]^T[D_\varphi]\{\bar{\varphi}\}dA \tag{34}$$

The equation of strain-displacement is used to the above equation as follow:

$$\begin{aligned}\Pi^M=&\frac{1}{2}\int_A\left\{\left([D_b^L]+\tfrac{1}{2}[D^N(w)]\right)\{\bar{u}\}\right\}^T[C]\left\{\left([D_b^L]+\tfrac{1}{2}[D^N(w)]\right)\{\bar{u}\}\right\}dA\\&+\frac{1}{2}\int_A\left(\{T\}^T-\{\bar{\varphi}\}^T[D_\varphi]^T[S_e]\right)\left([S]^{-1}\right)^T\left(\{T\}-[S_e]^T[D_\varphi]\{\bar{\varphi}\}\right)dA\\&+\frac{1}{2}\int_A\left\{[D_b^L]+\tfrac{1}{2}[D^N(w)]\{\bar{u}\}\right\}^T[C_e]^T\{\bar{\varphi}\}dA\\&-\frac{1}{2}\int_A\left(\{T\}^T-\{\bar{\varphi}\}^T[D_\varphi]^T[S_e]\right)\left([S]^{-1}\right)^T[S_e]^T[D_\varphi]\{\bar{\varphi}\}dA\end{aligned} \tag{35}$$

The electric energy can be defined as follow:

$$\Pi^P=\frac{1}{2}\int_V\{\nabla\varphi\}^T\{D^u\}dV+\frac{1}{2}\int_V\{\nabla\varphi\}^T\{D^\varphi\}dV \tag{36}$$

Where Π^P, is the electric energy, , the gradient of electric potential , $\{D^u\}$, the vector of the piezoelectric electric displacement, $\{D^\varphi\}$, the vector of the dielectric electric displacement.
The volume integral is replaced to the surface integral as follow.

$$\Pi^P=\int_A\int_{-h/2}^{+h/2}\sum_{\rho=1}^{NP}\left(\left\{[Z_\varphi^\rho][D_\varphi^\rho]\{\varphi^\rho(x,y)\}\right\}^T\left\{\begin{matrix}\frac{1}{2}\left[\begin{array}{c|c}[0] & [\bar{e}_s]\\ \hline \{\bar{e}_p\}^T & <0>\end{array}\right]_\rho\begin{Bmatrix}\{\varepsilon_p\}\\ \hline \{\varepsilon_s\}\end{Bmatrix}_\rho\\ -\frac{1}{2}\left[\begin{array}{c|c}[\mu_s] & \{0\}\\ \hline <0> & \mu_p\end{array}\right]_\rho[Z_\varphi^\rho][D_\varphi^\rho]\{\varphi^\rho(x,y)\}\end{matrix}\right)dz\,dA \tag{37}$$

The follow equation is obtained by the coefficient matrix.

$$\Pi^P=\frac{1}{2}\int_A\{\bar{\varphi}\}^T[C_e]\{\varepsilon_b\}dA+\frac{1}{2}\int_A\{[D_\varphi]\{\bar{\varphi}\}\}^T[S_e]\{\varepsilon_s\}dA-\frac{1}{2}\int_A\{[D_\varphi]\{\bar{\varphi}\}\}^T[C_\mu][D_\varphi]\{\bar{\varphi}\}dA \tag{38}$$

The equation of strain-displacement is used as follow.

$$\begin{aligned}\Pi^P=&\frac{1}{2}\int_A\left\{\left([D_b^L]+\tfrac{1}{2}[D^N(w)]\right)\{\bar{u}\}\right\}^T[C_e]^T\{\bar{\varphi}\}dA\\&+\frac{1}{2}\int_A\left(\{\hat{T}\}-[S_e]^T[D_\varphi]\{\bar{\varphi}\}\right)^T\left([S_e][S]^{-1}\right)^T\{[D_\varphi]\{\bar{\varphi}\}\}dA\\&-\frac{1}{2}\int_A\{\bar{\varphi}\}^T\left([C_\mu][D_\varphi]\right)^T\{[D_\varphi]\{\bar{\varphi}\}\}dA\end{aligned} \tag{39}$$

The electric matrix of layer is defined as follow:

$$[C_\mu]=\mathrm{diag}\left[[C_\mu]_1\cdots[C_\mu]_{NP}\right]$$
$$[C_\mu]_\rho=\int_{z_\rho}^{z_{\rho+1}}[Z_\varphi^\rho]^T[\mu]_\rho[Z_\varphi^\rho]dz=\begin{bmatrix}[\mu_{11}] & [\mu_{12}] & [0]\\ [\mu_{21}] & [\mu_{22}] & [0]\\ [0] & [0] & [\mu_{33}]\end{bmatrix}_\rho \tag{40}$$
$$(i,j=1,2)\Rightarrow[\mu_{ij}]_\rho=\frac{(\mu_{ij})_\rho\,t_\rho}{6}\begin{bmatrix}2 & 1\\ 1 & 2\end{bmatrix}$$
$$[\mu_{33}]_\rho=\frac{(\mu_{33})_\rho}{t_\rho}\begin{bmatrix}1 & -1\\ -1 & 1\end{bmatrix}$$

The displacement field, the electric potential and the transverse shear stress are described by two dimension elements. The element parameters are defined as follow:

$$\{\bar{u}^e\} = [N_u]\{\hat{u}^e\}$$
$$[N_u] = \begin{bmatrix} N_1[I_5] & N_2[I_5] & \cdots & N_n[I_5] \end{bmatrix}$$
$$\{\hat{u}^e\} = \begin{bmatrix} \{\hat{u}^e\}_1 \ldots & \{\hat{u}^e\}_n \end{bmatrix}^T$$
$$\{\bar{\varphi}^e\} = [N_\varphi]\{\hat{\varphi}^e\}$$
$$\{\hat{\varphi}^e\} = \begin{bmatrix} \{\hat{\varphi}^e\}_1 \ldots & \{\hat{\varphi}^e\}_n \end{bmatrix}^T$$
$$[N_\varphi] = \begin{bmatrix} [\hat{N}_{\varphi 1}] & [\hat{N}_{\varphi 2}] & \cdots & [\hat{N}_{\varphi n}] \end{bmatrix}$$
$$[\hat{N}_{\varphi i}] = \begin{bmatrix} N_i & 0 & \cdots & 0 \\ 0 & N_i & \cdots & 0 \\ 0 & N_i & \cdots & 0 \\ \vdots & \vdots & \ddots & \vdots \\ 0 & 0 & \cdots & N_i \end{bmatrix}_{2NP\,x\,(NP+1)} \quad (41)$$

Where N_i, is the shape function of node i^{th}, $[\hat{N}_{\varphi i}]$, the shape function matrix of electric potential, , $[I_5]$, unit matrix 5×5, n, the number of shape functions, $\{\hat{u}^e\}_i$, the displacement vector, $\{\hat{\varphi}^e\}_i$, the potential vector of element e of node i. For i=5 to n, the shape functions are hierarchical functions.

By using lagrangian shape functions, the transverse shear stress T_{yz}^e and T_{XZ} are obtained.

$$\{\hat{T}^e\} = \begin{Bmatrix} \hat{T}_{yz}^e \\ \hat{T}_{xz}^e \end{Bmatrix} = \quad (42)$$
$$\begin{bmatrix} \bar{N}_1[I_2] & \bar{N}_2[I_2] & \cdots & \bar{N}_n[I_2] \end{bmatrix} \begin{Bmatrix} \{\hat{T}^e\}_1 \\ \{\hat{T}^e\}_2 \\ \vdots \\ \{\hat{T}^e\}_n \end{Bmatrix} = [N_T]\{\hat{T}^e\}$$

Where $\bar{N}_i$, is the shape function i^{th} transverse shear stress point, $\{\hat{T}^e\}_i$ the vector of transverse shear stress of i^{th} point of element e.

According to the follow equation, the combination of the mechanical and electrical energy functions presents the total energy function.

$$\Pi^e = \{\hat{u}^e\}^T \left[\frac{1}{2}\int_a \{[B_b^L] + \frac{1}{2}[B^N(w)]\}^T [C] \{[B_b^L] + \frac{1}{2}[B^N(w)]\} da \right] \{\hat{u}^e\}$$
$$+ \{\hat{u}^e\}^T \left[\int_a [B_s]^T [N_T] da \right] \{\hat{T}^e\} - \{\hat{T}^e\}^T \left[\frac{1}{2}\int_a [N_T][S]^{-1}[N_T]^T da \right] \{\hat{T}^e\}$$
$$+ \{\hat{u}^e\}^T \left[\int_a \{[B_b^L] + \frac{1}{2}[B^N(w)]\}^T [C_e]^T [N_\varphi] da \right] \{\hat{\varphi}^e\}$$
$$+ \{\hat{T}^e\}^T \left[\int_a [N_T]^T [S]^{-1} [S_e]^T [B_\varphi] da \right] \{\hat{\varphi}^e\}$$
$$- \{\hat{\varphi}^e\}^T \left[\frac{1}{2}\int_a \left([B_\varphi]^T [S_e][S]^{-1}[S_e]^T [B_\varphi] + [B_\varphi]^T [C_\mu][B_\varphi] \right) da \right] \{\hat{\varphi}^e\} \quad (43)$$

Where $[B_b^L]$, $[B_s]$, $[B^N]$ and $[B_\varphi]$ are the strain-displacement and the electric displacement-potential matrixes, Π^e, the total energy function, a, the area of element. These matrixes are defined as follow:

$$[B_b^L] = [D_b^L][N_u] = [[B_{b1}^L] \quad \cdots \quad [B_{bn}^L]]$$
$$[B_{bi}^L] = \begin{bmatrix} [B_{\varepsilon i}] & \{0\}_{3x1} & [0]_{3x2} \\ [0]_{3x2} & \{0\}_{3x1} & [B_{\vartheta i}] \end{bmatrix}$$
$$[B_{\varepsilon i}] = [D_\varepsilon][N_{Ni}] \qquad [B_{\vartheta i}] = [D_\vartheta][N_{Ni}] \quad (44)$$
$$[N_{Ni}] = \begin{bmatrix} N_i & 0 \\ 0 & N_i \end{bmatrix}$$
$$[B_s] = [D_s][N_u] = [[B_{s1}] \quad [B_{s2}] \quad \cdots \quad [B_{sn}]]$$
$$[B_{si}] = \begin{bmatrix} [0]_{2x2} & \{D_w\}N_i & -N_i[I_s] \end{bmatrix}$$

$$[B^N] = [D^N][N_u] = [[B_1^N] \quad [B_2^N] \quad \cdots \quad [B_n^N]] \quad [B_i^N(w)]$$
$$= \begin{bmatrix} [\Gamma_\theta(w)] \\ [0]_{3x2} \end{bmatrix} [G]_i \quad (45)$$
$$[\Gamma_\theta(w)] = \begin{bmatrix} \Gamma_1 & 0 \\ 0 & \Gamma_2 \\ \Gamma_2 & \Gamma_1 \end{bmatrix} \quad \Gamma_1 = \left[\frac{\partial N}{\partial x}\right]\{w\}, \quad \Gamma_2 = \left[\frac{\partial N}{\partial y}\right]\{w\}$$
$$[G]_i = \begin{bmatrix} 0 & 0 & \frac{\partial N_i}{\partial x} & 0 & 0 \\ 0 & 0 & \frac{\partial N_i}{\partial y} & 0 & 0 \end{bmatrix}$$
$$\left[\frac{\partial N}{\partial x}\right] = \left[\frac{\partial N_1}{\partial x} \; \frac{\partial N_2}{\partial x} \; \ldots\ldots \frac{\partial N_n}{\partial x}\right]$$

$$[B_\varphi] = [D_\varphi][N_\varphi] = \left[[D_\varphi][\hat{N}_{\varphi 1}] \quad \ldots [D_\varphi][\hat{N}_{\varphi n}]\right] \quad (46)$$

According to the variation method of the energy function, the follow equation is obtained.

$$
\begin{aligned}
&\delta\Pi^{e} = \\
&\left\{\delta\hat{u}^{e}\right\}^{T}\left[\int_{a}\{[B_{b}^{L}]+[B^{N}(w)]\}^{T}[C]\left([B_{b}^{L}]+\tfrac{1}{2}[B^{N}(w)]\right)da\right]\{\hat{u}^{e}\} \\
&+\left\{\delta\hat{u}^{e}\right\}^{T}\left[\int_{a}[B_{s}]^{T}[N_{Q}]\,da\right]\{\hat{T}^{e}\}+<\delta\hat{T}^{e}>\left[\int_{a}[N_{Q}]^{T}[B_{s}]\,da\right]\{\hat{u}^{e}\} \\
&-\left\{\delta\hat{T}^{e}\right\}^{T}\left[\int_{a}[N_{Q}][S]^{-1}[N_{Q}]^{T}\,da\right]\{\hat{T}^{e}\} \\
&+\left\{\delta\hat{u}^{e}\right\}^{T}\left[\int_{a}\{[B_{b}^{L}]+[B^{N}(w)]\}^{T}[C_{e}]^{T}[N_{\varphi}]\,da\right]\{\hat{\varphi}^{e}\} \\
&+\left\{\delta\hat{\varphi}^{e}\right\}^{T}\left[\int_{a}[N_{\varphi}]^{T}[C_{e}]\left([B_{b}^{L}]+\tfrac{1}{2}[B^{N}(w)]\right)da\right]\{\hat{u}^{e}\} \\
&+\left\{\delta\hat{T}^{e}\right\}^{T}\left[\int_{a}[N_{Q}]^{T}[S]^{-1}\left([S_{e}]^{T}[B_{\varphi}]\right)da\right]\{\hat{\varphi}^{e}\} \\
&+\left\{\delta\hat{\varphi}^{e}\right\}^{T}\left[\int_{a}[B_{\varphi}]^{T}[S_{e}][S]^{-1}[N_{Q}]\,da\right]\{\hat{T}^{e}\} \\
&-\left\{\delta\hat{\varphi}^{e}\right\}^{T}\left[\int_{a}\left([B_{\varphi}]^{T}[S_{e}][S]^{-1}[S_{e}]^{T}[B_{\varphi}]+[B_{\varphi}]^{T}[C_{\mu}][B_{\varphi}]\right)da\right]\{\hat{\varphi}^{e}\}=0
\end{aligned}
\tag{47}
$$

The kinetic energy function J^{e} and the virtual work due to the mechanical and electrical loading W^{e} are expressed as follow 0:

$$
J^{e}=\frac{1}{2}\int_{V}\rho\left\{\hat{u}^{e}\right\}^{T}\left[N_{u}\right]^{T}\left[N_{u}\right]\left\{\hat{u}^{e}\right\}dV \tag{48}
$$

$$
W^{e}=\left\{\hat{u}^{e}\right\}^{T}\int_{V}\left[N_{u}\right]^{T}\left\{f^{u}\right\}dV+\left\{\hat{\varphi}^{e}\right\}^{T}\int_{V}\left[N_{\varphi}\right]^{T}\left\{f^{\varphi}\right\}dV \tag{49}
$$

By using Hamilton equation and the method of variation, the equation of motion is obtained as follow:

$$
\begin{bmatrix}[M] & 0 & 0\\ 0 & 0 & 0\\ 0 & 0 & 0\end{bmatrix}_{e}\begin{Bmatrix}\{\hat{\ddot{u}}^{e}\}\\ \{\hat{\ddot{\varphi}}^{e}\}\\ \{\hat{\ddot{T}}^{e}\}\end{Bmatrix}+ \tag{50}
$$

$$
\left(\begin{bmatrix}[K^{uu}] & [K^{u\varphi}] & [K^{uT}]\\ [K^{\varphi u}] & [K^{\varphi\varphi}] & [K^{\varphi T}]\\ [K^{Tu}] & [K^{T\varphi}] & [K^{TT}]\end{bmatrix}_{e}+\begin{bmatrix}[K_{N}^{uu}] & [K_{N}^{u\varphi}] & [0]\\ [K_{N}^{\varphi u}] & [0] & [0]\\ [0] & [0] & [0]\end{bmatrix}_{e}\right)\begin{Bmatrix}\{\hat{u}^{e}\}\\ \{\hat{\varphi}^{e}\}\\ \{\hat{T}^{e}\}\end{Bmatrix}=
$$

$$
\begin{Bmatrix}\{f^{u}\}\\ \{f^{\varphi}\}\\ \{0\}\end{Bmatrix}
$$

$$
[K^{uu}]_{e}=\int_{a}[B_{b}^{L}]^{T}[C][B_{b}^{L}]da
$$

$$
[K^{uT}]_{e}=[K^{Tu}]_{e}^{T}=\int_{a}[B_{s}]^{T}[N_{T}]da
$$

$$
[K^{TT}]_{e}=-\int_{a}[N_{T}][S]^{-1}[N_{T}]^{T}da
$$

$$
[K^{u\varphi}]_{e}=[K^{\varphi u}]_{e}^{T}=\int_{a}[B_{b}^{L}]^{T}[C_{e}]^{T}[N_{\varphi}]da
$$

$$
[K^{T\varphi}]_{e}=[K^{\varphi T}]_{e}^{T}=\int_{a}[N_{T}]^{T}[S]^{-1}\left([S_{e}]^{T}[B_{\varphi}]\right)da
$$

$$
[K^{\varphi\varphi}]_{e}=-\int_{a}[B_{\varphi}]^{T}[S_{e}][S]^{-1}[S_{e}]^{T}[B_{\varphi}]da-\int_{a}[B_{\varphi}]^{T}[C_{\mu}][B_{\varphi}]da
$$

$$
[K_{N}^{uu}]_{e}=\int_{a}\begin{pmatrix}[B_{b}^{L}][C]\left(\frac{1}{2}[B^{N}(w)]\right)+[B^{N}(w)]^{T}[C][B_{b}^{L}]\\ +[B^{N}(w)]^{T}[C]\left(\frac{1}{2}[B^{N}(w)]\right)\end{pmatrix}da
$$

$$
[K_{N}^{u\varphi}]_{e}=\int_{a}[B^{N}(w)]^{T}[C_{e}]^{T}[N_{\varphi}]da
$$

$$
[K_{N}^{\varphi u}]_{e}=\int_{a}[N_{\varphi}]^{T}[C_{e}]\left(\tfrac{1}{2}[B^{N}(w)]\right)da
$$

$$
[M]=\int_{V}[N_{u}]^{T}\,\rho[N_{u}]dV
$$

Where $\{f^{u}\}_{e}$, is the mechanical load vector, $\{f^{\varphi}\}_{e}$, the electrical load vector of element e.

The vibration modes of a plate have strain nodes. In this nodes, the strain sign changes in the plate width and length. It is demonstrated that the phenomena of voltage cancellation is obtained by the strain nodes in the vibration modes. The segmented electrodes can be used for preventing the voltage cancellation.

This paper investigates the cancellation phenomenon observed in the voltage response of piezoelectric harvesters. The analysis considers a bimorph plate configuration with both continuous and segmented electrodes. The constitutive equation relating the electric current and the electrical field in a piezoelectric layer is derived from Gauss's law, which can be expressed as:

$$
\frac{d}{dt}\left(\int_{A}D.ndA\right)=\frac{v(t)}{R_{l}} \tag{51}
$$

Where R_l, is resistive load, v, electric potential, n, unit normal, D, electric displacement vector and A, electrode area.

If the plate is thin and the nonlinear strain parameter in equation is omitted, the axial strains will be proportional to the plate curvature at level 'z'.

$$
\varepsilon_{x}\approx-z\frac{\partial^{2}w(x,y,t)}{\partial x^{2}}\qquad\varepsilon_{y}\approx-z\frac{\partial^{2}w(x,y,t)}{\partial y^{2}}\qquad\gamma_{xy}\approx-z\frac{\partial^{2}w(x,y,t)}{\partial x\,\partial y} \tag{52}
$$

By using the piezoelectric constitutive relationship, the following equation is obtained.

$$
D_{z}=\begin{bmatrix}\bar{e}_{31} & \bar{e}_{32} & \bar{e}_{36}\end{bmatrix}\begin{Bmatrix}\varepsilon_{x}\\ \varepsilon_{y}\\ \gamma_{xy}\end{Bmatrix}+\mu_{33}E_{z}\qquad E_{z}(t)=\frac{-v(t)}{2h_{p}} \tag{53}
$$

$$C_p^{eq}\frac{dv(t)}{dt}+\frac{v(t)}{R_l}=-e_{31}\frac{h_p}{2}\int_A\frac{\partial^3 w_{rel}(x,y,t)}{\partial x^2\partial t}dA- \\ e_{32}\frac{h_p}{2}\int_A\frac{\partial^3 w_{rel}(x,y,t)}{\partial y^2\partial t}dA-e_{36}\frac{h_p}{2}\int_A\frac{\partial^3 w_{rel}(x,y,t)}{\partial y\,\partial x\,\partial t}dA \quad (54)$$

$$C_p^{eq}=\mu_{33}\frac{A}{2h_p}$$

According to above equation, the bending slope at the electrodes boundaries is an effective factor in the harvester. For a certain mode shape, If the sign of the strain distribution changes, the phenomena of the electrical cancellation from the energy harvesting will obtain for a certain vibration mode.

The Eigen curvature function reveals the conditions leading to voltage cancellation. The presence of both negative and positive regions under the Eigen curvature function results in a reduction of electrical output due to the integration of electric displacement. Therefore, using segmented electrodes and integrating only over specific electrode areas can mitigate this cancellation phenomenon.

The locations where the curvature changes sign are referred to as strain nodes. These strain nodes correspond to the inflection points of the Eigen curvature function for a given vibration mode.

3. Properties of specimen

The used piezoelectric plate is PZT-5A in the series connection. The specimen was obtained from Piezo System. Its properties are presented in Table 2. Fig. 4 shows the connection type of the piezoelectric layers.

The cases of boundary conditions are as: Clamp in the all edges of plate(cccc), Simply support in the all edges of plate(ssss), Two Simply supports and clamps in the edges of plate(scsc). The Fig. 5 shows the position of boundary conditions.

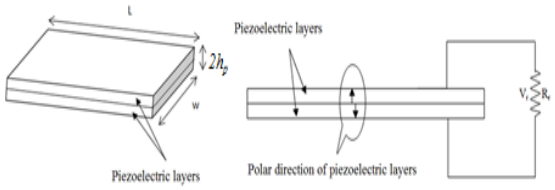

Fig. 4. The type of connection of piezoelectric layers.

Table 2. The properties of piezoelectric plate. dimensions.

W(m)	$2h_p$(m)	L(m)
1×10^{-1}	1×10^{-3}	1×10^{-1}

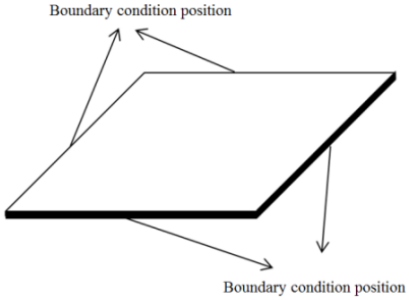

Fig. 5. The position of boundary condition.

By using a finite element method for piezoelectric nonlinear plate in the Matlab software, the electrical response of plate is obtained. The harmonic excitation force is applied for the electrical response by the follow equation. The excitation acceleration is considered 9.81(m/s^2).

$$F=2\rho h_p a_e \cos(\omega t) \quad (55)$$

Where ρ, is the density of piezoelectric plate, a a_e , the amplitude of excitation acceleration, ω, the excitation force frequency, h_p, the layer thickness and t, time.

4. Results and discussion

The voltage response of the piezoelectric nonlinear plate is shown in Figs. 6 and 7 for limitation of the first and second frequency. As is clear from the figure, the behavior of voltage with frequency is nonlinear. In physical terms, this means that with the same frequency changes, the behavior of the voltage response of the structure is not the same on both sides of the natural frequency.

According to the results, the case of simply support in all edges of the plate has the maximum voltage. The case of clamp in all edges of the plate has the minimum voltage response in the open circuit condition.

The first frequencies of maximum voltage response for clamps, simply supports and simply supports-clamps boundary conditions are 549, 415 and 263Hz, respectively, and the second frequencies of maximum voltage response are 1687, 881 and 809Hz, respectively.

By comparing the obtained results with the results of reference 0, it can be seen that in the case of the sheet model with supporting restraints on both sides, the resulting voltage has increased about two times. Due to the fact that the model of this research has two sides and the

reference model 0 has one support side, the effect of the increase in voltage obtained by increasing the supports was taken into consideration.

The mode shapes for the clamp boundary conditions are shown in Figs. 8 and 9. The mode shapes for the simply supports boundary conditions are shown in Figs. 10 and 11. Figs. 12 and 13 present the mode shapes for the clamp-simply supports boundary conditions.

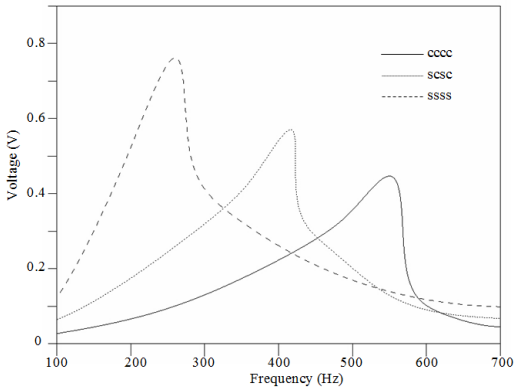

Fig. 6. The voltage response of piezoelectric nonlinear plate in the limitation of the first mode.

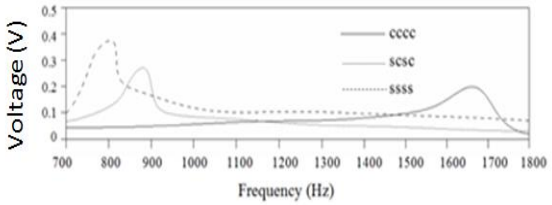

Fig. 7. The voltage response of piezoelectric nonlinear plate in the limitation of the second mode.

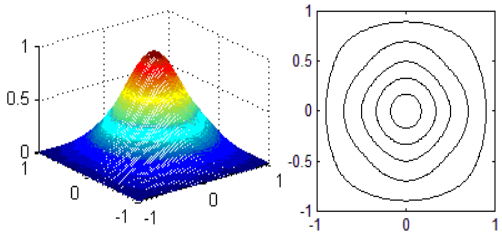

Fig. 8. The first mode shape for the clamp boundary conditions**.**

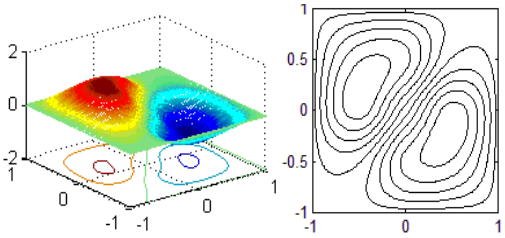

Fig. 9. The second mode shape for the clamp boundary conditions**.**

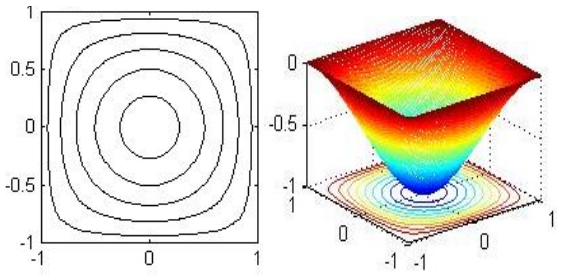

Fig. 10. The first mode shape for the simply supports boundary conditions.

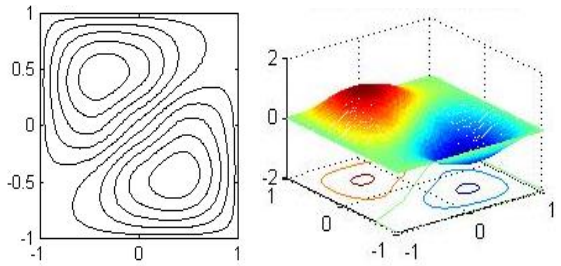

Fig. 11. The second mode shape for the simply supports boundary conditions.

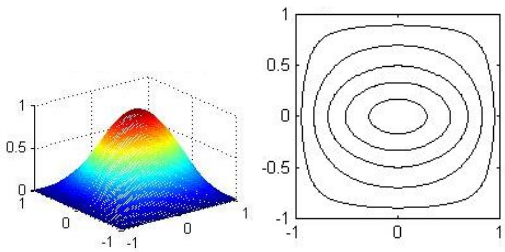

Fig. 12. The first mode shapes for the clamp-simply supports boundary conditions.

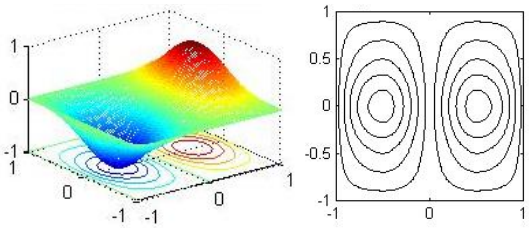

Fig. 13. The second mode shapes for the clamp-simply supports boundary conditions.

The curvature of electrodes is one of the effective parameters in the response of voltage. The change of curvature in the mode shape causes the change of voltage phase. In the finite element model, the strain elements have the strain nodes. In these elements, the curvature direction changes and, the strain is zero. The Fig. 14 shows the strain elements.

The nodes with the phase angle φ is shown by symbol ● and the phase angle φ+180 by symbol ○. The strain elements have the both of nodes.

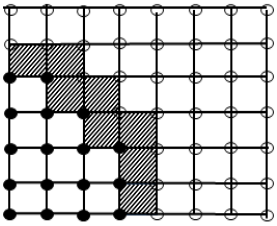

Fig. 14. The strain elements.

These elements are the boundary of potential region and the position of separated electrodes. Fig. 15 shows the change of the plate curvature direction in the clamp boundary conditions for the first mode shape. The finite element model has two segmented electrodes. Each segment has the steady electrical potential. (Fig. 16)

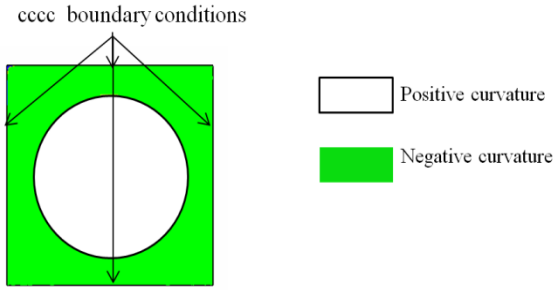

Fig. 15. The change of the plate curvature direction for the clamp boundary conditions in the first mode shape.

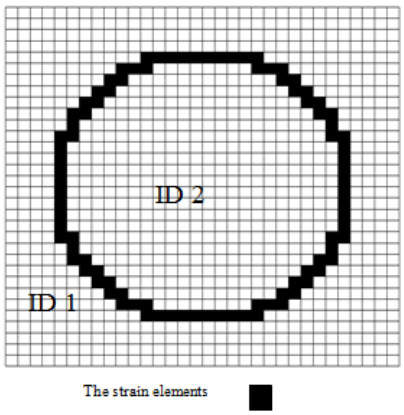

Fig. 16. The separated electrodes in the clamp boundary conditions for the first mode shape.

The voltage results in the case of the segmented electrodes are shown in Fig. 17 for clamp boundary conditions and frequency 549Hz. The response of voltage for the continuous electrode and the combination of segmented electrodes are shown in Fig. 18.

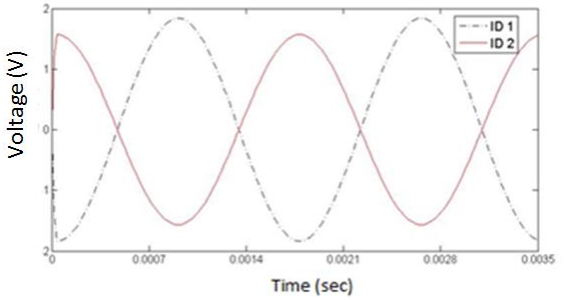

Fig. 17. The voltage results in the case of the segmented electrodes.

The voltage amplitude for frequency 549Hz is 0.49V in clamp boundary conditions and the continuous electrode, while this voltage is 3.16V in the combination of separated electrodes.

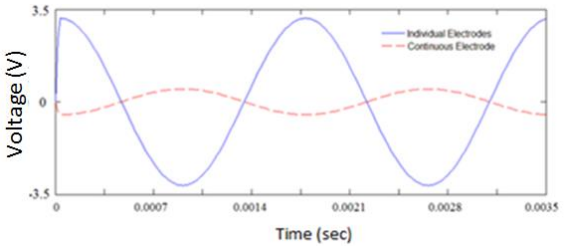

Fig. 18. The response of voltage for the continuous electrodes case and the combination of segmented electrodes.

The change of the plate curvature direction is shown in Fig. 19 for simply support boundary conditions in the first mode shape. The finite element model has two segmented electrodes(Fig. 20).
The voltage results in the case of the segmented electrodes are shown in Fig. 21 for simply supports boundary condition and frequency 263Hz. The response of voltage for the continuous electrodes and combination of segmented electrodes are shown in Fig. 22.

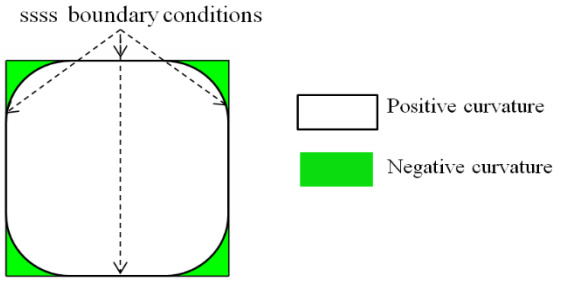

Fig. 19. The change of the plate curvature direction for simply supports boundary conditions in the first mode shape.

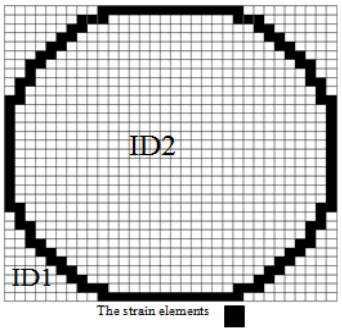

Fig. 20. The separated electrodes in simply supports boundary conditions for the first mode shape.

The voltage amplitude for frequency 263Hz is 0.77V in simply supports conditions and the continuous electrode, while this voltage is 1.3V in the separated electrodes.

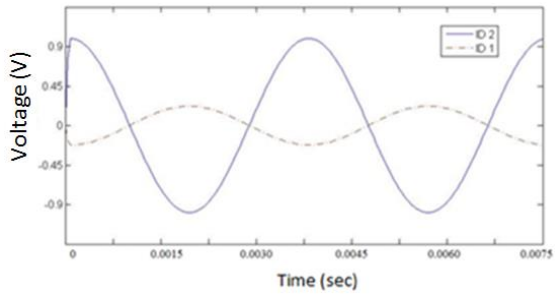

Fig. 21. The results of voltage in the case of the segmented electrodes for simply supports boundary condition.

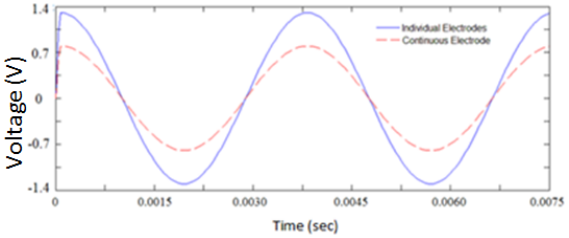

Fig. 22. The response of voltage for the continuous electrodes case and combination of segmented electrodes.

The change of the plate curvature direction is shown in Fig. 23 for simply-clamp boundary conditions in the first mode shape. The finite element model has two segmented electrodes (Fig. 24).

By comparing the results with reference 0, it can be seen that in the case of the sheet model, with the presence of supporting supports on both sides of the sheet model, the resulting voltage is much higher than that of the single-support beam in reference 0. This result shows that the application of the sheet model using the strain node separation method and the presence of two supporting supports will have an effective effect on increasing the voltage response.

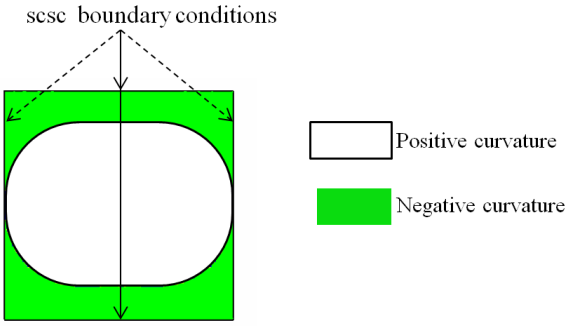

Fig. 23. The change of the plate curvature direction for simply-clamp boundary conditions in the first mode shape.

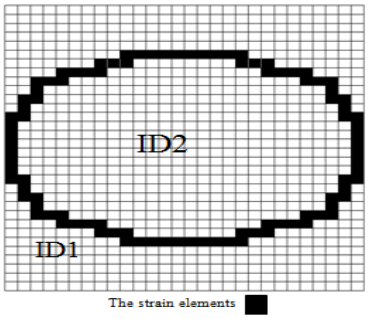

Fig. 24. The separated electrodes in the finite element model for simply-clamp boundary conditions in the first mode shape.

The voltage results in the case of the segmented electrodes are shown in Fig. 25 for simply-clamp boundary conditions and frequency 415Hz. The response of voltage for the continuous electrodes and combination of segmented electrodes are shown in Fig. 26.

The voltage amplitude for frequency 415Hz is 0.56V in simply support-clamp conditions and the continuous electrode, while this voltage is 2.7V in the separated electrodes. The result of all cases is been shown in Fig. 27.

According to the results, the maximum of voltage response is related to clamp boundary conditions in the segmented electrode and the minimum of voltage response is related to clamp boundary conditions in the continuous electrode. The voltage response for different boundary condition cases is shown in the Table 3.

The obtained results can be compared with the results presented in reference 0. In reference 0, the beam type structure is 40mm long, and in the continuous electrode state, the voltage response is about 0.25V, and in this research, the plate type structure with a length of 100mm has the voltage response of 0.5V. Comparing these two researches, the result is suitable for the

continuous electrode mode and this research shows that by using the individual electrode, a significant increase in the voltage response is obtained.

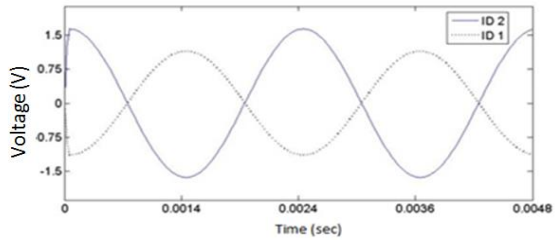

Fig. 25. The voltage results in the case of the segmented electrodes for simply-clamp boundary condition and frequency 415Hz.

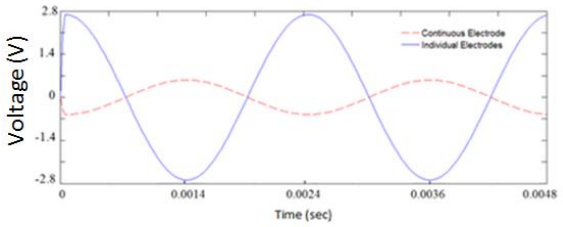

Fig. 26. The response of voltage for the continuous electrode case and combination of segmented electrodes.

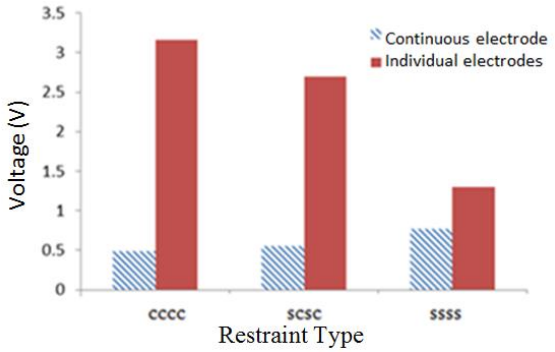

Fig. 27. The result of all cases.

Table 3. The result of Voltage responsible for variable boundary condition

B.C	Frequency(Hz)	Continuous Electrode Voltage(V)	Individual Electrode Voltage(V)
ssss	263	0.77	1.3
scsc	415	0.56	2.7
cccc	549	0.49	3.16

5. Conclusions

This paper investigates the electrical response of a piezoelectric nonlinear plate, specifically focusing on a bimorph configuration under various boundary conditions and in an open-circuit state. The analysis demonstrates that the presence of strain nodes, inherent in the vibration modes of the plate, significantly influences voltage output due to the cancellation effect. The vibration modes have strain nodes.

The piezoelectric plate was used in both the continuous electrode and the segmented electrode example.

This research investigated the electrical response of the open-circuit case under harmonic excitation. Improved energy harvesting performance was observed using separated electrodes. The Mindlin plate theory and Von Kármán strain were employed in the analysis. Harvester behavior was examined under various boundary conditions.

In all cases, the voltage response for the continuous electrode was lower than that for the segmented electrodes at the first natural frequency.

This suggests a significant difference in how the continuous and segmented electrodes respond to the same excitation (presumably vibration or some other external force) under clamped-clamped boundary conditions. The segmented electrode's peak response under these conditions implies a more efficient concentration or transfer of the excitation energy, while the continuous electrode's minimum response indicates a less effective energy transfer or dissipation. Further investigation is needed to understand the underlying mechanisms.

References

[1] E. Hausler, L. Stein, and G. Harbauer, "Implantable physiological power supply with PVDF film", *J. Ferroelectrics*, Vol. 60, No. 1, pp. 277–282, (1984).

[2] M. Lallart, S.R Anton, DJ. Inman, "Frequency self-tuning scheme for broadband vibration energy harvesting", *J. Intell. Mater. Syst. Struct.*, Vol. 21, No. 9, pp. 897–906, (2010).

[3] A. Erturk, D.J. Inman, "Assumed-modes formulation of piezoelectric energy harvesters: euler-bernoulli, rayleigh and timoshenko models with axial deformations", *Proceedings of the ASME*, ESDA 10th Biennial Conference on Engineering Systems, Design and Analysis, (2010).

[4] A. Erturk, D. Inman, "Piezoelectric energy harvesting", John Wiley & Sons, (2011).

[5] A. Erturk, *Electromechanical modelling of piezoelectric energy harvesters. Dissertation*, PhD thesis, Virginia Polytechnic Institute and State University, (2009).

[6] M. Jabbari, M. Ghayour and H.R. Mirdamadi, "Energy harvesting of a multilayer piezoelectric beam in resonance and off-resonance cases", *J. Eng. Mater. Technol.*, Vol. 139, *No.3,pp.* 031008, (2017).

[7] M. Kogl and M.L. Bucalem, "Analysis of smart laminates using piezoelectric MITC plate and shell elements", *J. Comput. Struct.*, Vol. 83, No. 15, pp. 1163-1153, (2005).

[8] C, Bendigeri, R. Tomar, S. Basavaraju and K. Arasukumar, "Detailed formulation and programming method for piezoelectric finite element", *Int. J. Pure Appl. Sci. Technol*, Vol. 7, No. 1, pp. 1-21, (2011).

[9] G. Sebald, H. Kuwano and D. Guyomar, "Experimental duffing oscillator for broadband piezoelectric energy harvesting", *J. Smart Mater. Struct.*, Vol. 20, No. 10, pp. 1–10, (2011).

[10] V. Piefor and, A. Preumont, "Modeling of smart piezoelectric structures with finite elements", *ISMA25*, 25th International Conference on Noise and Vibration Engineering, Leuven, Belgium, (2000).

[11] A. Erturk and D. Inman, "Broadband piezoelectric power generation on high-energy orbits of the bistable duffing oscillator with electromechanical coupling", *J. Sound Vib.*, Vol. 330, No. 10, pp. 2339–2353, (2011).

[12] D. Van, P. Dealmeida and S. Vander Zwaag, "Piezoelectric and mechanical properties of novel composites of PZT and a liquid crystalline thermosetting resin", *J. Mater Sci*., Vol. 42, pp. 6417–6425, (2007).

[13] P. Brian and S. Senthil, "Active vibration suppression of sandwich beams using piezoelectric shear actuators: experiments and numerical simulations", *J. Intell. Mater. Syst. Struct.*, Vol. 16, No. 6, pp. 518-521, (2005).

[14] M. Jabbari, M. Ghayour and H.R. Mirdamadi, "Experimental and numerical results of dynamics behavior of a nonlinear piezoelectric beam", *J. Mech. Adv. Mater. Struct.*, Vol. 23, No. 8, pp. 853-864, (2015).

[15] T. Ng and W. Liao, "Sensitivity analysis and energy harvesting for a self-powered piezoelectric sensor", *J. Intell. Mater. Syst. Struct.*, Vol. 16, No.10, pp. 785–797, (2005).

[16] A. Lazarus, O. Thomas and J. Deu, "Finite element reduced order models for nonlinear vibration of piezoelectric layered beams with applications to NEMS", *J. Finite Elem. Anal. Des.*, Vol. 49, No. 1, pp. 51-35, (2012).

[17] No. 0119620, *Multistage force amplification of piezoelectric stacks*, T. Xu, E. Siochi, L. Zuo, X. Jiang and JH. Kang, (2012).

[18] T. Xu, J. Emilie, J. Kang, L. Zuo, W. Zhou, X. Tang and X. Jiang, "Energy harvesting using a PZT ceramic multilayer stack", *J. Struct.*, Vol. 22, No. 6, pp. 065015, (2013).

[19] M. Kaltenbacher, "Finite element formulation for ferroelectric hysteresis of piezoelectric materials", *J. Intell. Mater. Syst. Struct.*, Vol. 21, No. 8, pp. 773–785, (2010).

[20] C. Yudong and Y. Bintang, "Non-linear modelling of multilayer piezoelectric actuators in non-trivial configurations based on actuator design parameters and piezoelectric material properties", *J. Intell. Mater. Syst. Struct.*, Vol. 23, No. 8, pp. 875–884, (2012).

[21] M. Jabbari, "The effect of strain nodes on the energy harvesting of the cantilever piezoelectric beam with the vibration mode excitation", *Modares Mechanical Engineering*, Vol. 17, No. 10, pp. 65-72, (2017).

[22] N. Kong, D.S. Ha, A. Erturk and D. Inman, "Resistive impedance matching circuit for piezoelectric energy harvesting", *J. Intell. Mater. Syst. Struct*, Vol. 21, No. 13, pp. 293–302, (2010).

[23] T. Xu, L. Tolliver, X. Jiang and J. Su, "A single crystal lead magnesium niobate-lead titanate multilayer-stacked cryogenic flextensional actuator", *J. Appl. Phys. Lett*, Vol. 102, No. 4, pp. 042906, (2013).

[24] S. Nurettin and K. Muammer, "A comprehensive review on the state-of-the-art of piezoelectric energy harvesting", *J. Nano Energy*, Vol. 80, No. 105567, (2021).

[25] Z. Xiaotian, H. Lipeng, W. Shuangjian , L. Xuejin, L. Renwen and C. Guangming, "A review of piezoelectric energy harvesters for harvesting wind energy", *J. Sens. Actuators, A.*, Vol. 352, No. 5, pp. 114190, (2023).

[26] J. Han, S.H. Park, and Y.S. Jung, "High-performance piezoelectric energy harvesting in amorphous perovskite thin films deposited directly on a plastic substrate", *J. Nat Commun*., Vol. 15, No.1, pp. 4129, (2024).

[27] A. Givois, C. Giraud-Audine, JF. Deü, "Experimental analysis of nonlinear resonances in piezoelectric plates with geometric nonlinearities", *Nonlinear Dyn*, Vol. 102, No. 1, pp. 1451–1462, (2020).

[28] A. Shariati, S.H.S. Hosseini, F. Ebrahimi, "Nonlinear dynamics and vibration of reinforced piezoelectric scale-dependent plates as a class of nonlinear Mathieu–Hill systems: parametric excitation analysis", *Engineering with Computers*, Vol. **37**, No. 1, pp. 2285–2301, (2021).

[29] H. Kuok, M. Stewart, A. Atanas and H.J Colin, " Performance of a cantilever piezoelectric energy harvester impacting bump stop", *J. Sound Vib.*, Vol. 330, No. 25, pp. 6184-6202, (2011).

[30] S. Beeby, M. Tudor and N. White, "Energy harvesting vibration sources for microsystems applications", *J. Meas. Sci. Technol.*, Vol. 17, No. 12, pp. 175–195,

[31] O. Zienkiewicz, *The Finite Element Method*, McGRAW-HILL Book Company, (1979).